Electronic Supplementary Material (ESI) for Journal of Materials Chemistry A.

Supporting Information

MOF surface method for ultrafast and one-step generation of metal-oxide-NP@MOF composite as lithium storage materials

Chang Sheng Yan,[a] Heng Ya Gao,[a] Le Le Gong,[a] Lu Fang Ma,*[b] Li Long Dang,[a,b] Le Zhang,[a] Pan Pan Meng,[a] and Feng Luo[a]*

This file includes:
Figure S1-22

Fig. S1 Single crystal x-ray structures of UTSA-74. a) The dinuclear unit built on both tetrahedral and octahedral Zn ions and its connectivity connecting to four identical organic ligands. b) The connectivity of the organic ligand that connects to four identical dinuclear units. Consequently, c) and d) the combination of dinuclear unit and organic ligands creates a fgl topology.

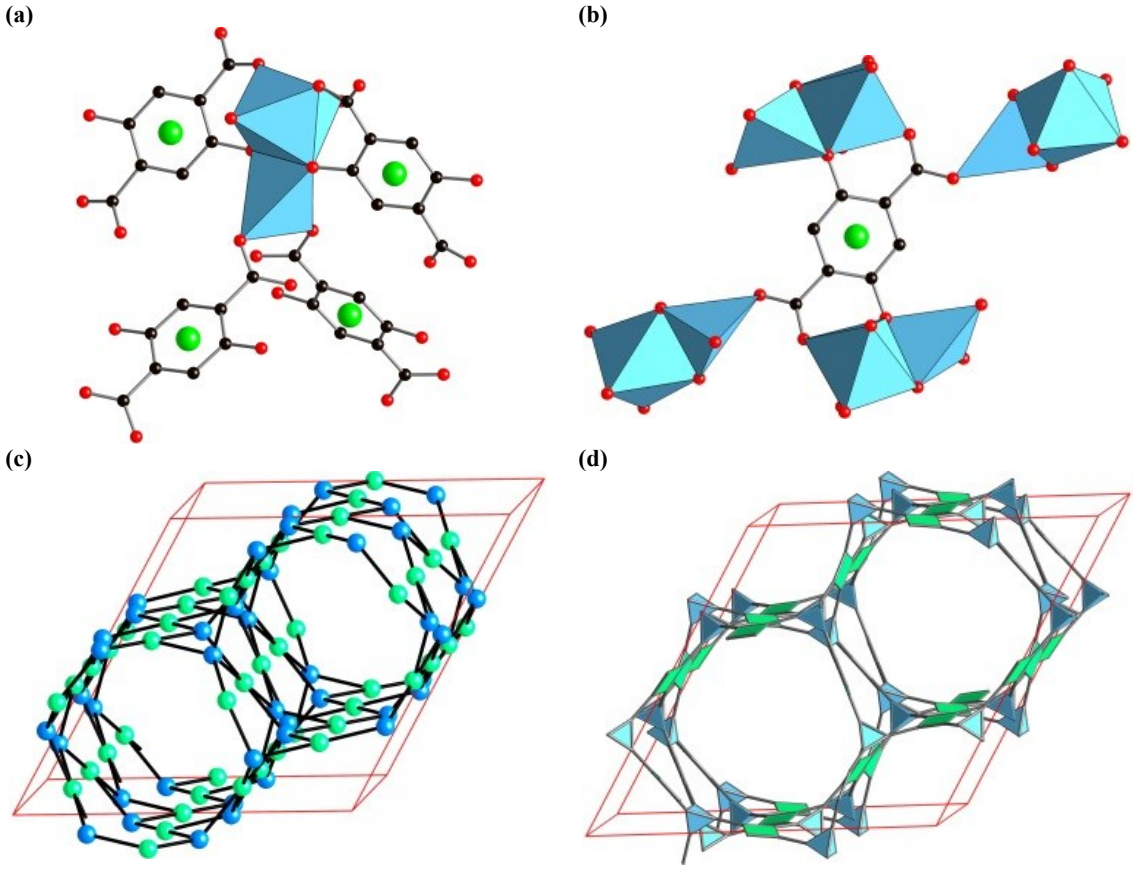

Fig. S2 Representative SEM, TEM and HRTEM images of Fe_2O_3@MOF-74. The Fe_2O_3 gives a leaves-like morphology.

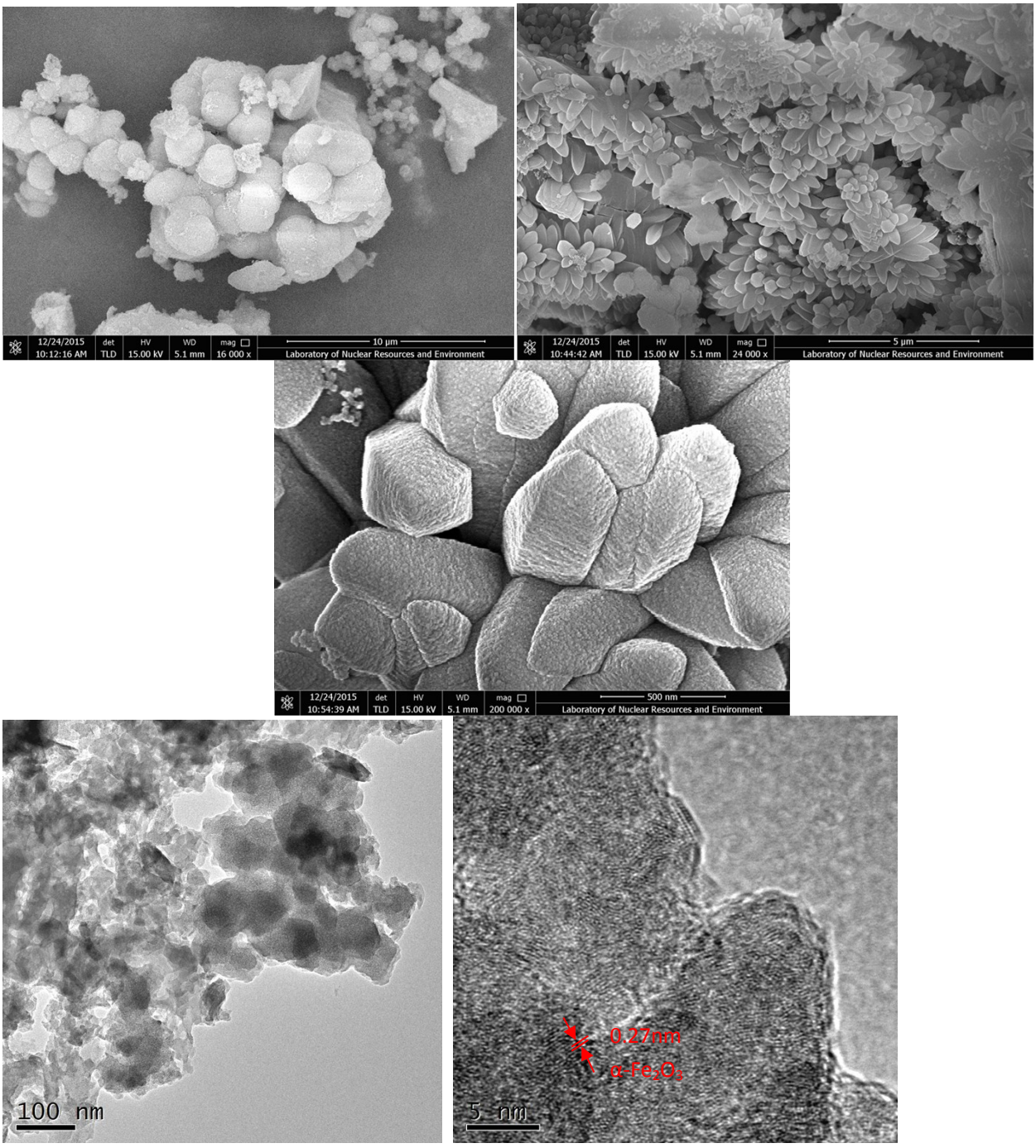

Fig. S3 Representative SEM, TEM and HRTEM images of Fe_2O_3@UTSA-74. The Fe_2O_3 gives a nanosheet morphology.

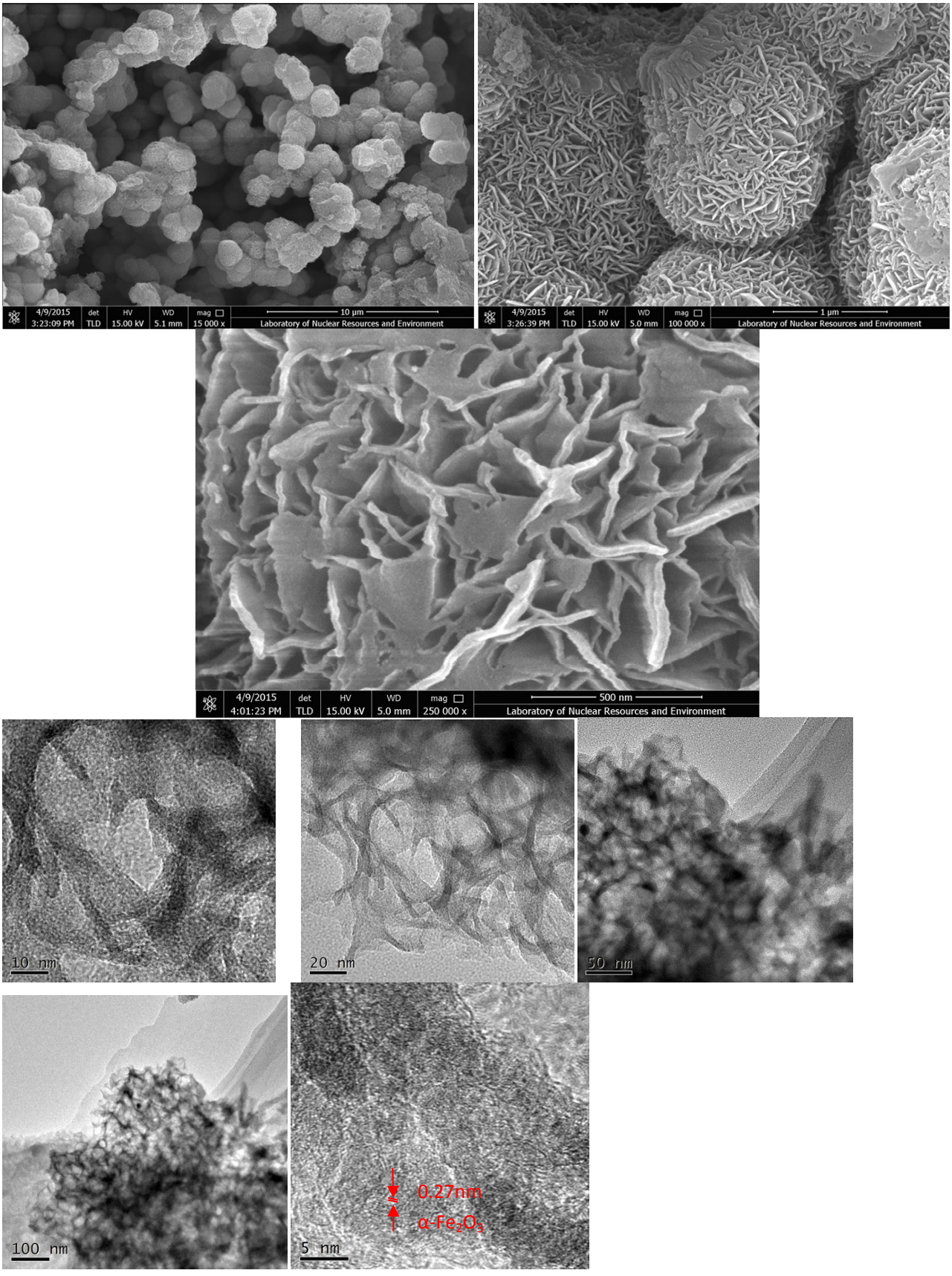

Fig. S4 Representative TEM, and HRTEM images of Fe_2O_3@ $Mg(DHT)(DMF)_2$.

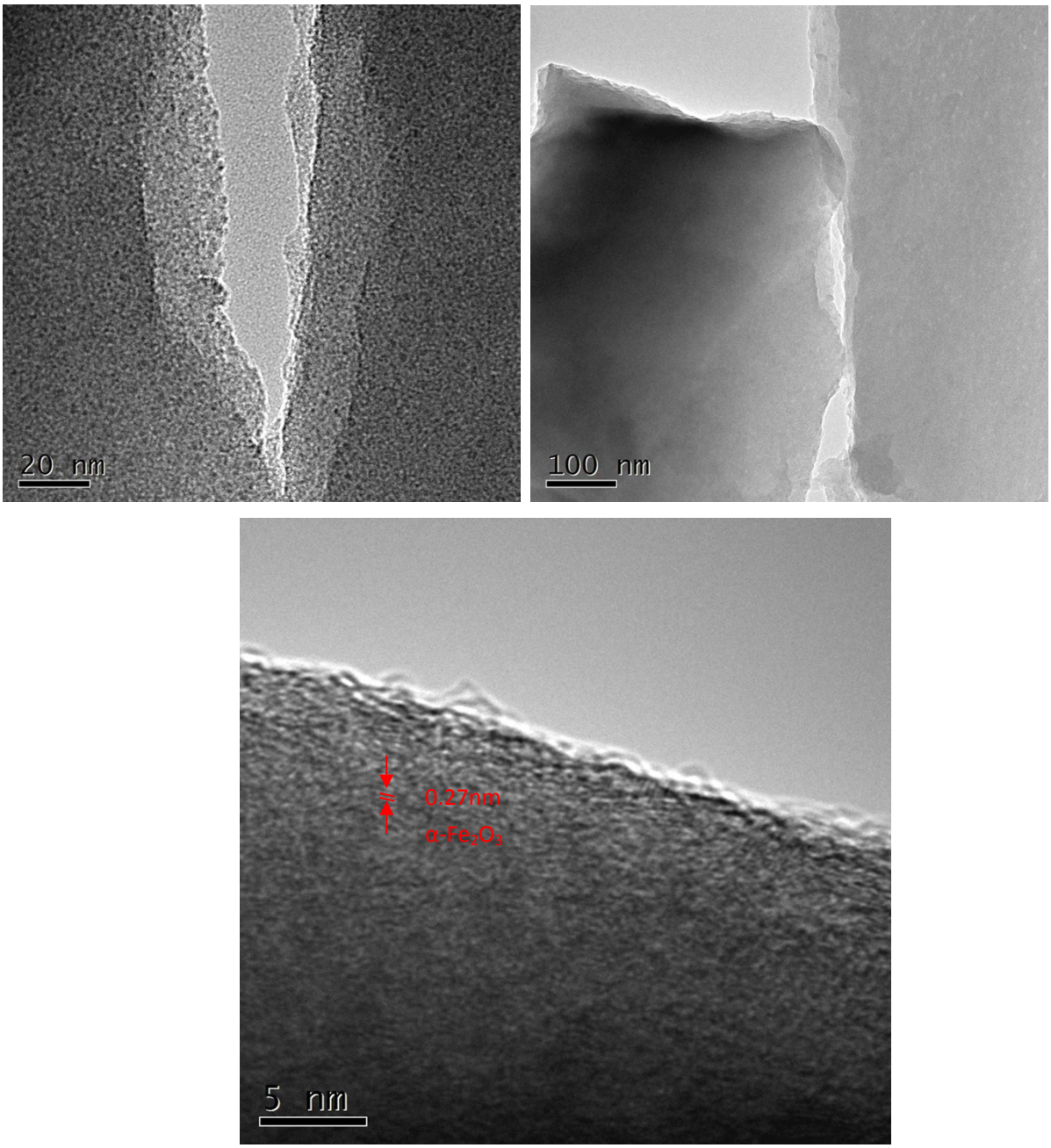

Fig. S5 Representative SEM images of as-synthesized UiO-66$(OH)_2$ samples and representative SEM, TEM, and HRTEM images of Fe_2O_3@ UiO-66$(OH)_2$, respectively. This clearly implies the as-synthesized UiO-66$(OH)_2$ samples in the form of nanoparticle and undetectable morphology for the Fe_2O_3 (most likely bulk Fe_2O_3).

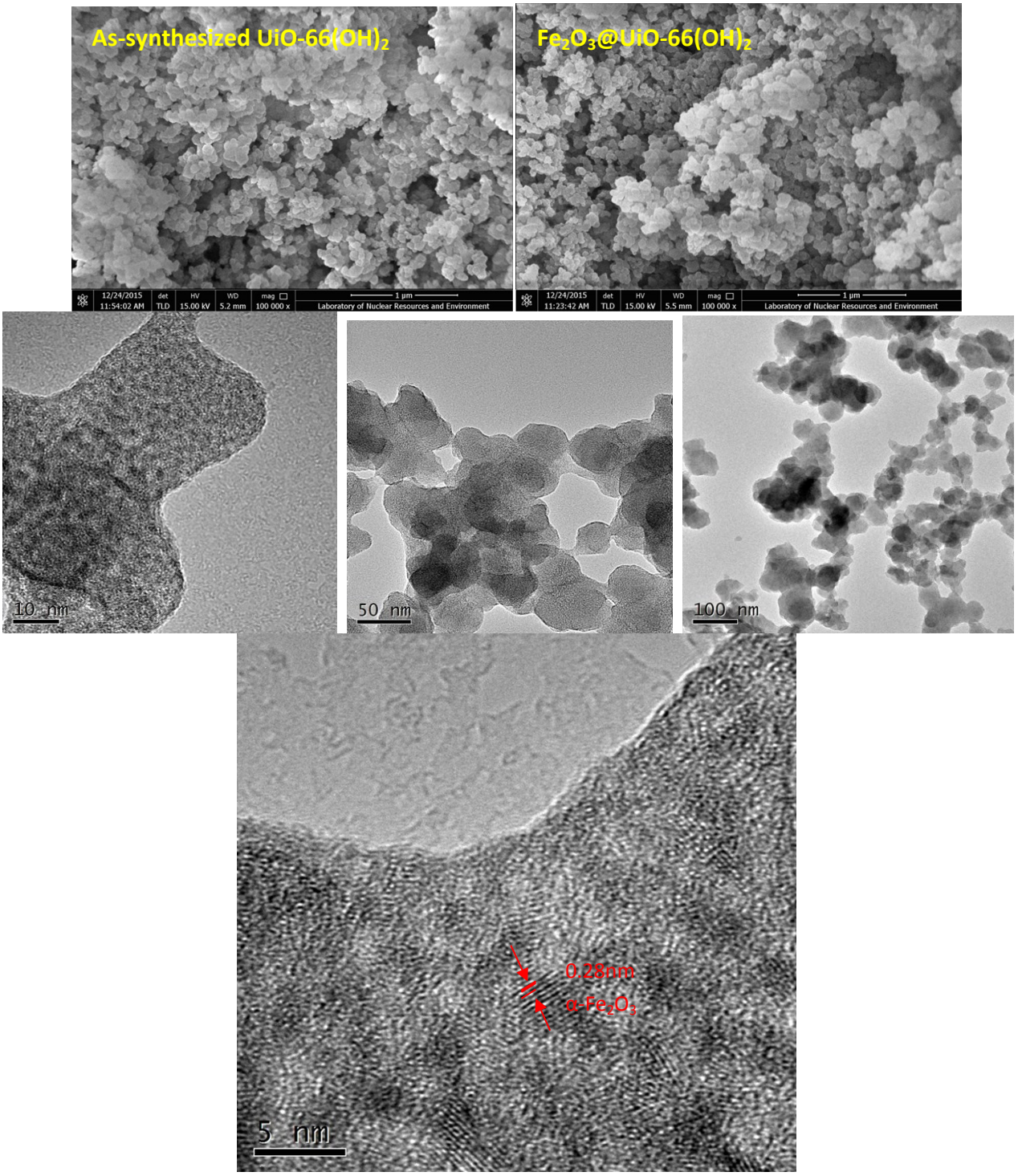

Fig. S6 Representative SEM images of as-synthesized UiO-66(OH) samples and representative SEM, TEM, and HRTEM images of Fe_2O_3@ UiO-66(OH), respectively. This clearly implies the as-synthesized UiO-66$(OH)_2$ samples in the form of nanoparticle and undetectable morphology for the Fe_2O_3 (most likely bulk Fe_2O_3).

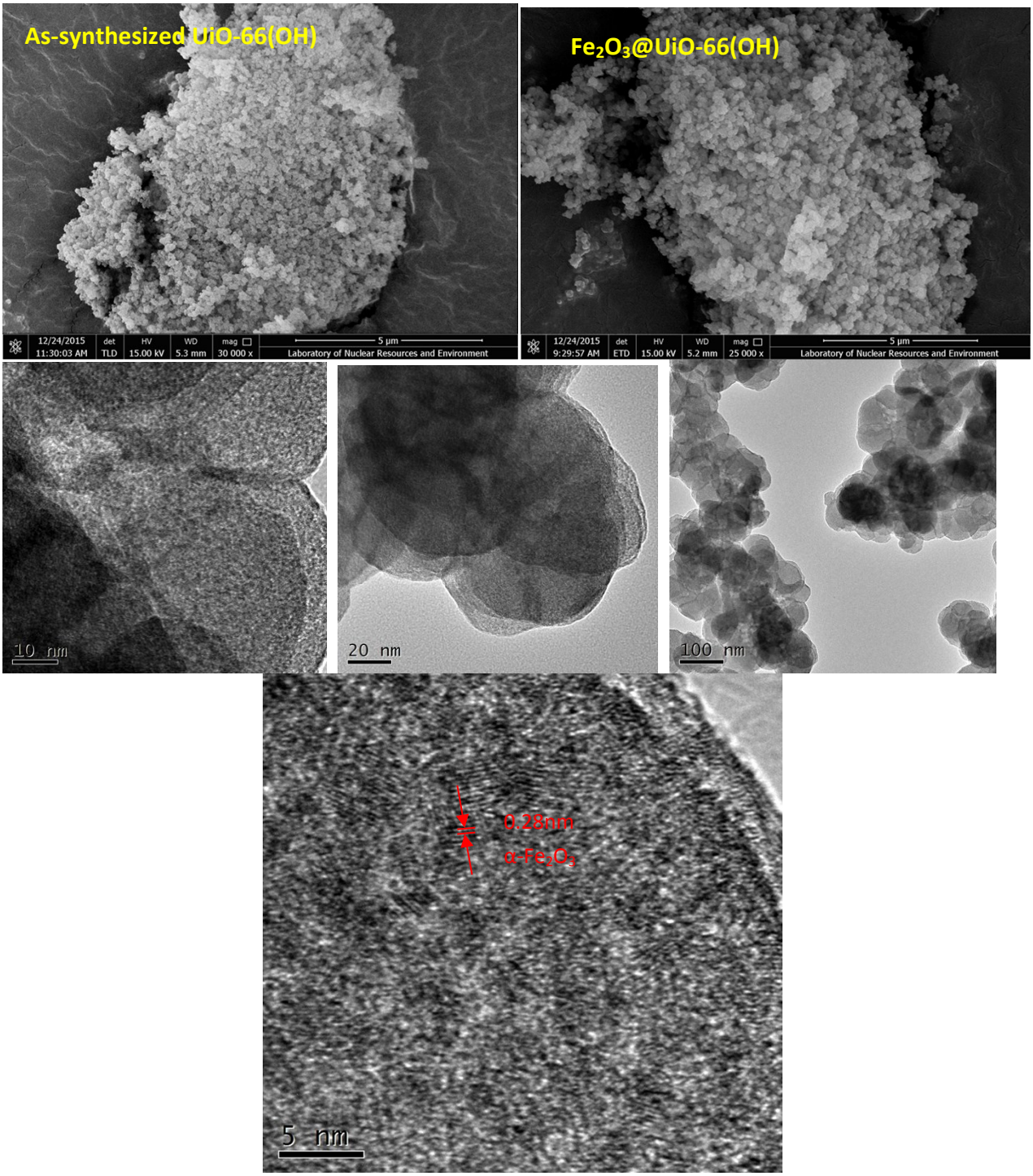

Fig. S7 IR bonds of as-synthesized MOF-74 samples and Fe_2O_3@MOF-74 composite. The difference between them is highlighted and derived from Fe_2O_3.

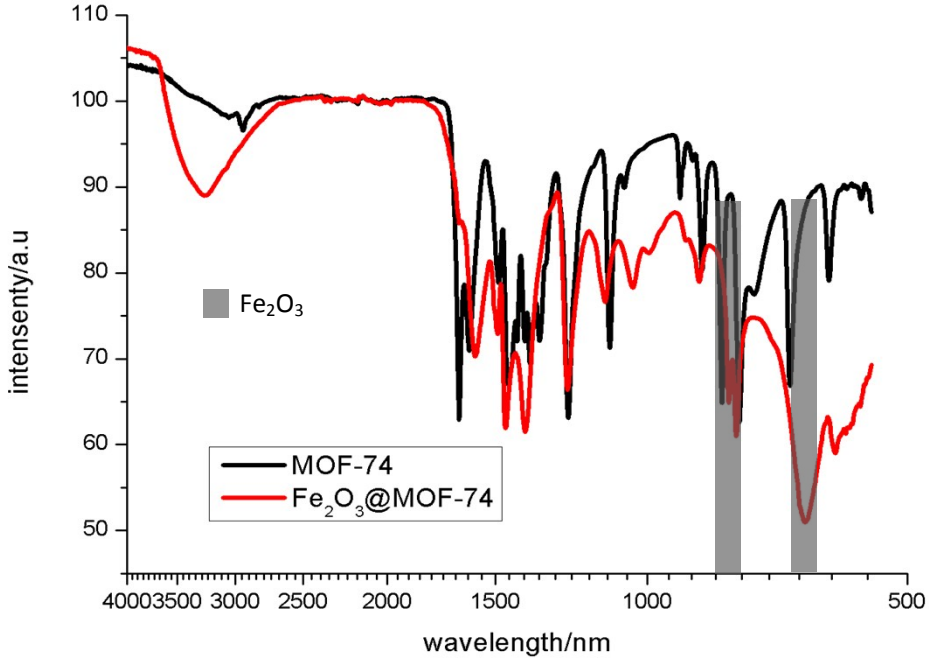

Fig. S8 IR bonds of as-synthesized UTSA-74 samples and Fe_2O_3@UTSA-74 composite. The difference between them is highlighted and derived from Fe_2O_3.

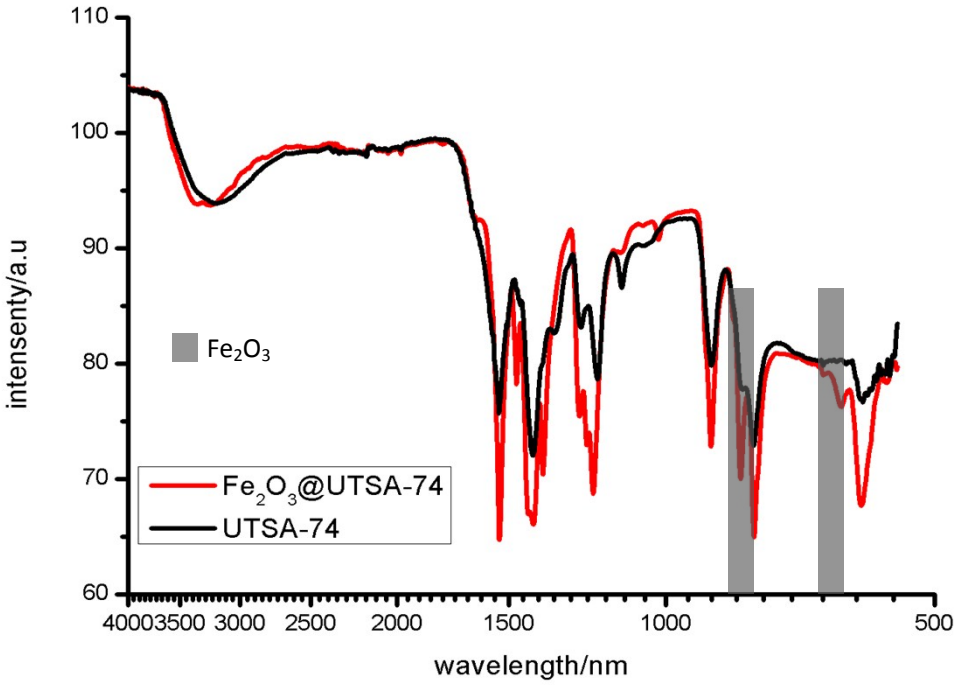

Fig. S9 IR bonds of as-synthesized $Mg(DHT)(DMF)_2$ samples and Fe_2O_3@$Mg(DHT)(DMF)_2$ composite. The difference between them is highlighted and derived from Fe_2O_3.

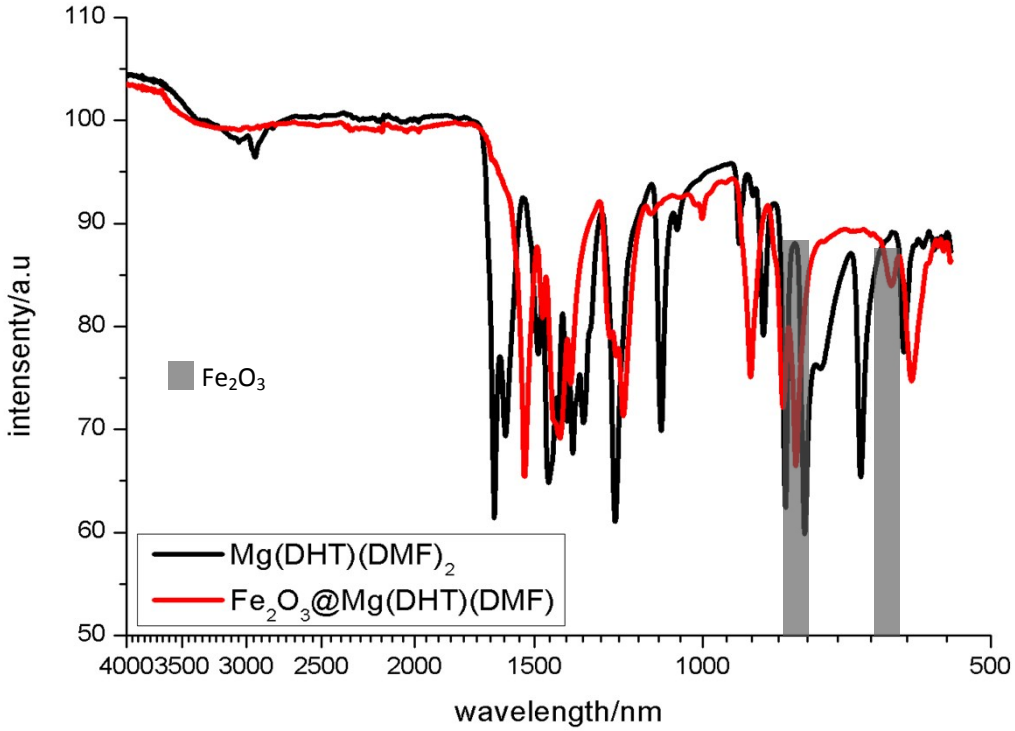

Fig. S10 IR bonds of as-synthesized UiO-66(OH)$_2$ samples and Fe_2O_3@UiO-66(OH)$_2$ composite. The difference between them is highlighted and derived from Fe_2O_3.

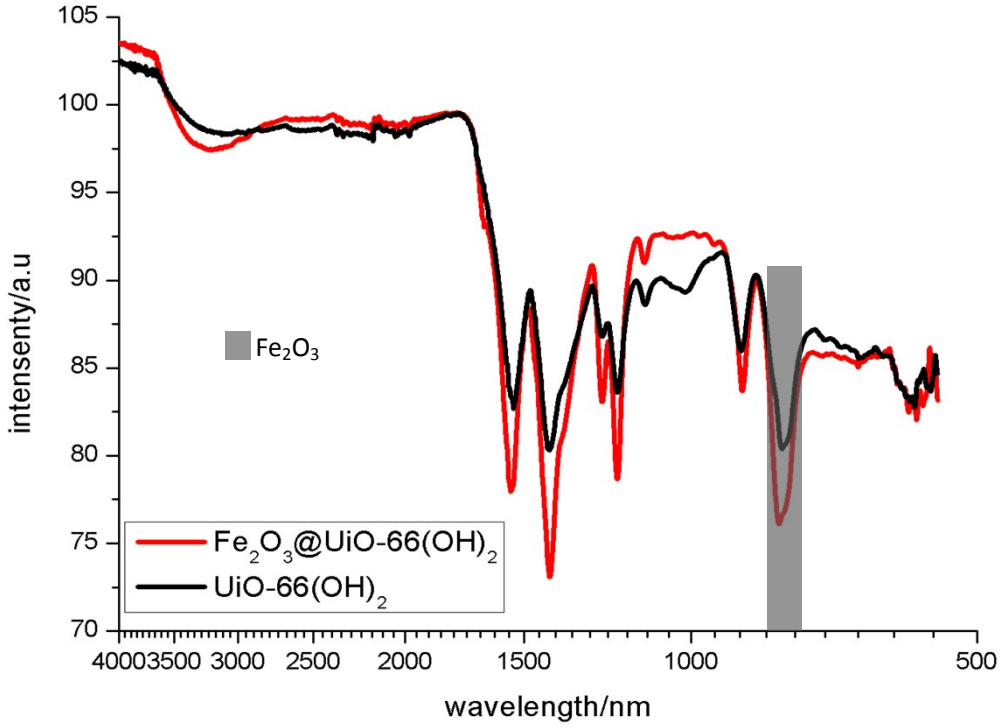

Fig. S11 IR bonds of as-synthesized UiO-66(OH) samples and Fe_2O_3@UiO-66(OH) composite. The difference between them is highlighted and derived from Fe_2O_3.

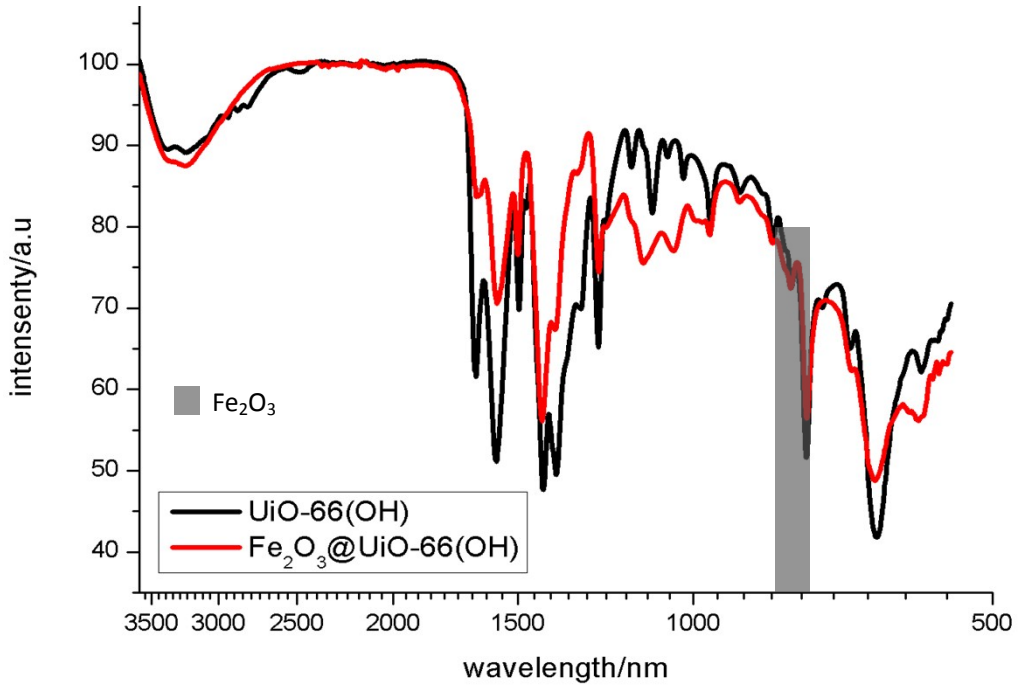

Fig. S12 XPS spectroscopy of Fe_2O_3@UTSA-74: F_{2p} (711, 719, 725, 734 eV) for Fe_2O_3 and O_{1s} (529.5, 531.6, 533.2 eV) for both Fe_2O_3 and UTSA-74.

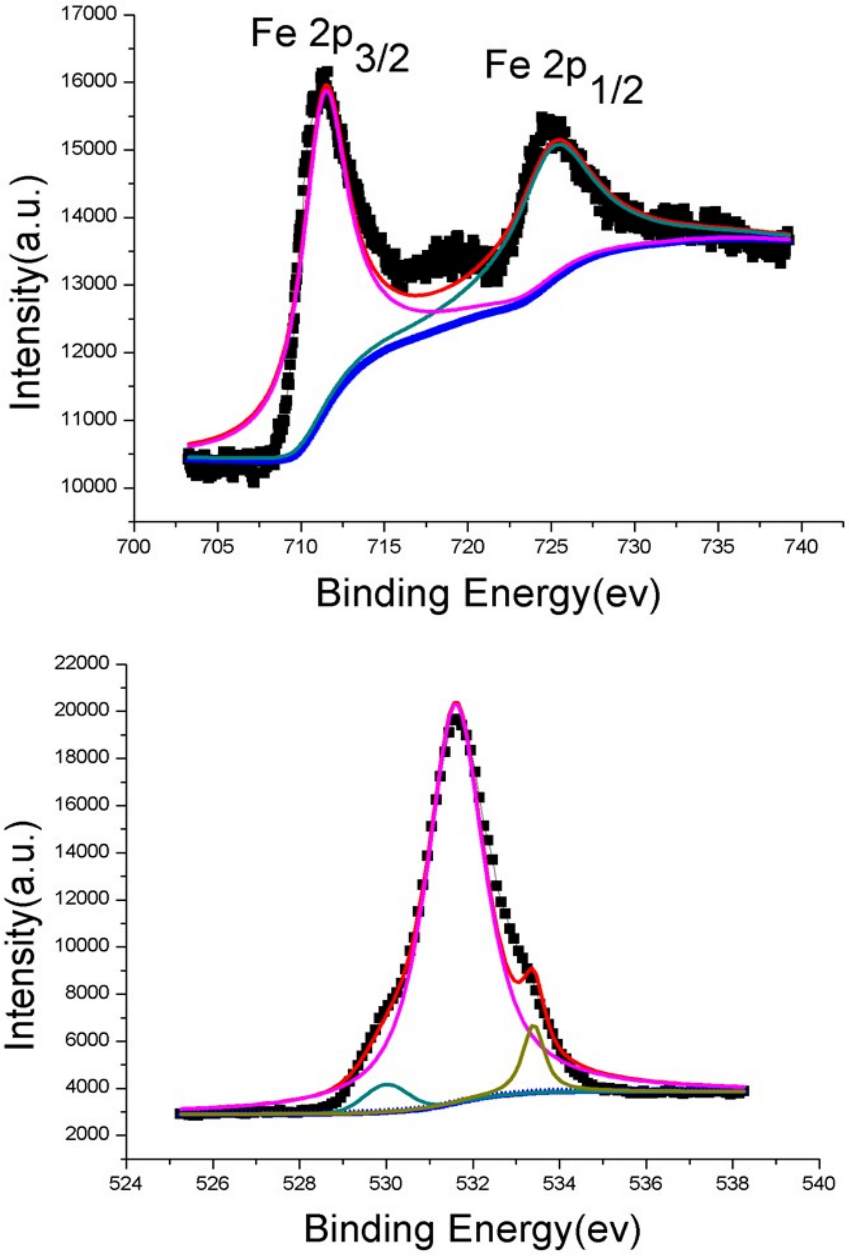

Fig. S13 XPS spectroscopy of Fe_2O_3@Mg(DHT)$(DMF)_2$: F_{2p} (712, 719, 726, 735 eV) for Fe_2O_3 and O_{1s} (530, 532, 533.5 eV) for both Fe_2O_3 and Mg(DHT)$(DMF)_2$

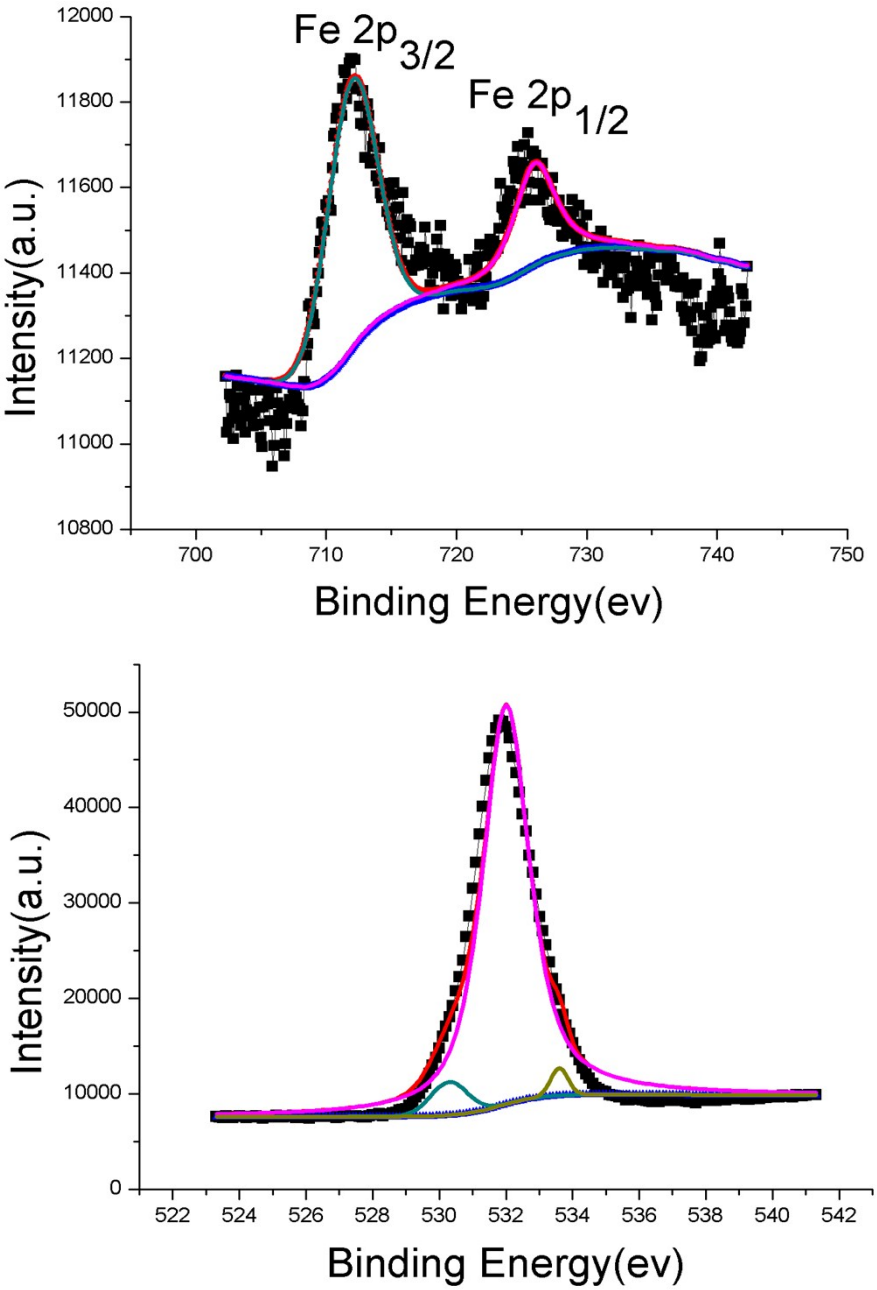

Fig. S14 XPS spectroscopy of Fe_2O_3@UiO-66(OH)$_2$: F_{2p} (711.7, 719, 725.8, 736 eV) for Fe_2O_3 and O_{1s} (530.2, 532, 533.5 eV) for both Fe_2O_3 and UiO-66(OH)$_2$.

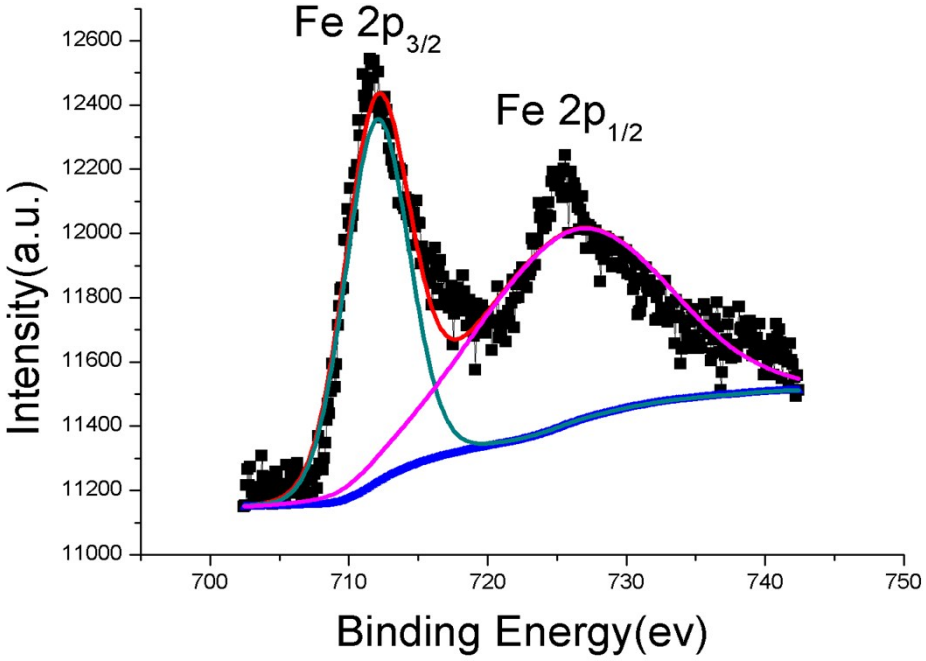

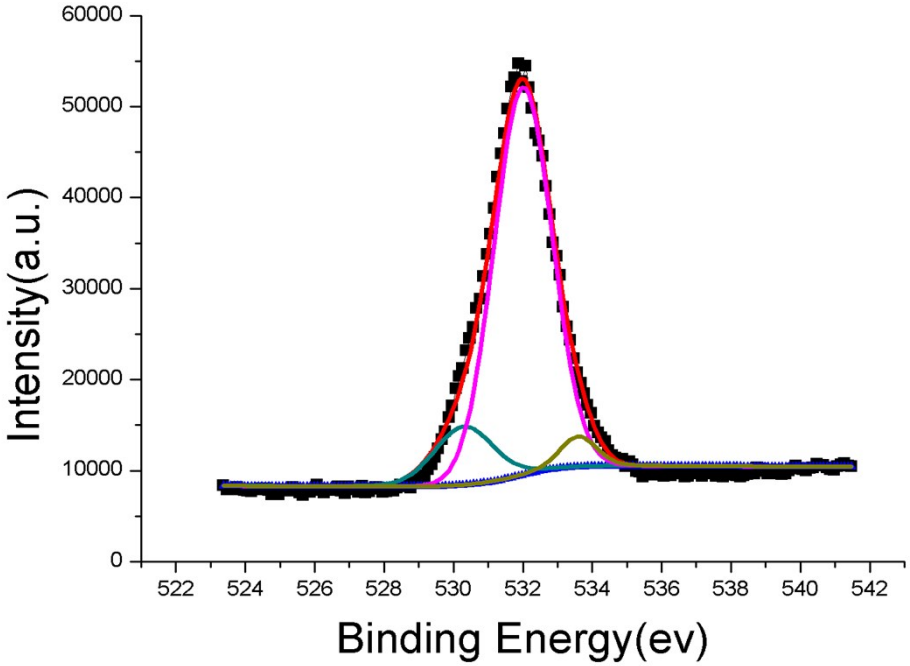

Fig. S15 XPS spectroscopy of Fe_2O_3@UiO-66(OH): F_{2p} (712, 718.5, 725.4, 735.4 eV) for Fe_2O_3 and O_{1s} (531.8, 533.5 eV) for both Fe_2O_3 and UiO-66(OH).

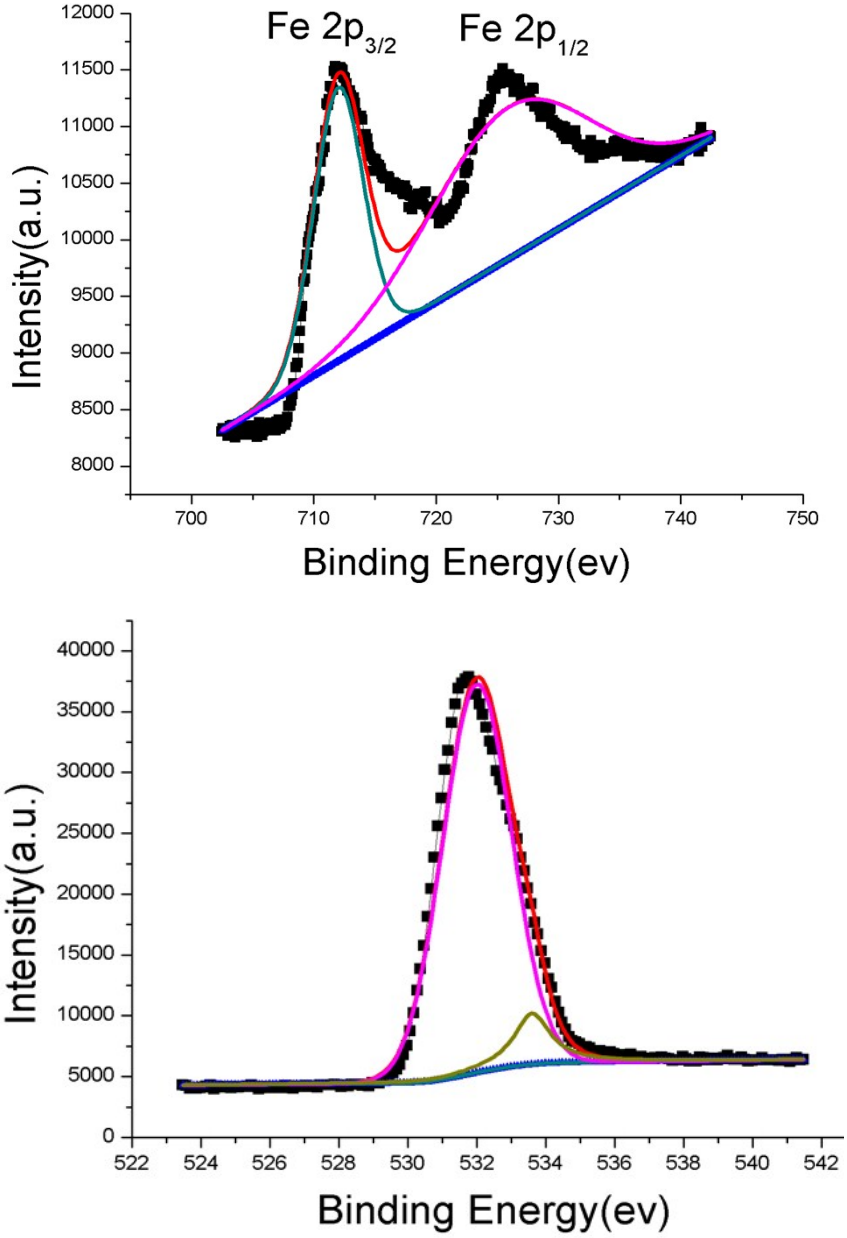

Fig. S16 Nitrogen physisorption isotherm of as-synthesized MOF-74 and Fe_2O_3@MOF-74 samples. The sample was pretreated at 80 °C under vacuum for 12 h. The BET surface area and Langmuir surface area for MOF-74 and Fe_2O_3@MOF-74 is 604/705.8 m^2/g and 13.2/15.6 m^2/g, respectively. MOF-74 gives aperture around 1.0 nm, comparable with the value in literature, whereas Fe_2O_3@MOF-74 creates mesoporous form with aperture around 11.3 nm.

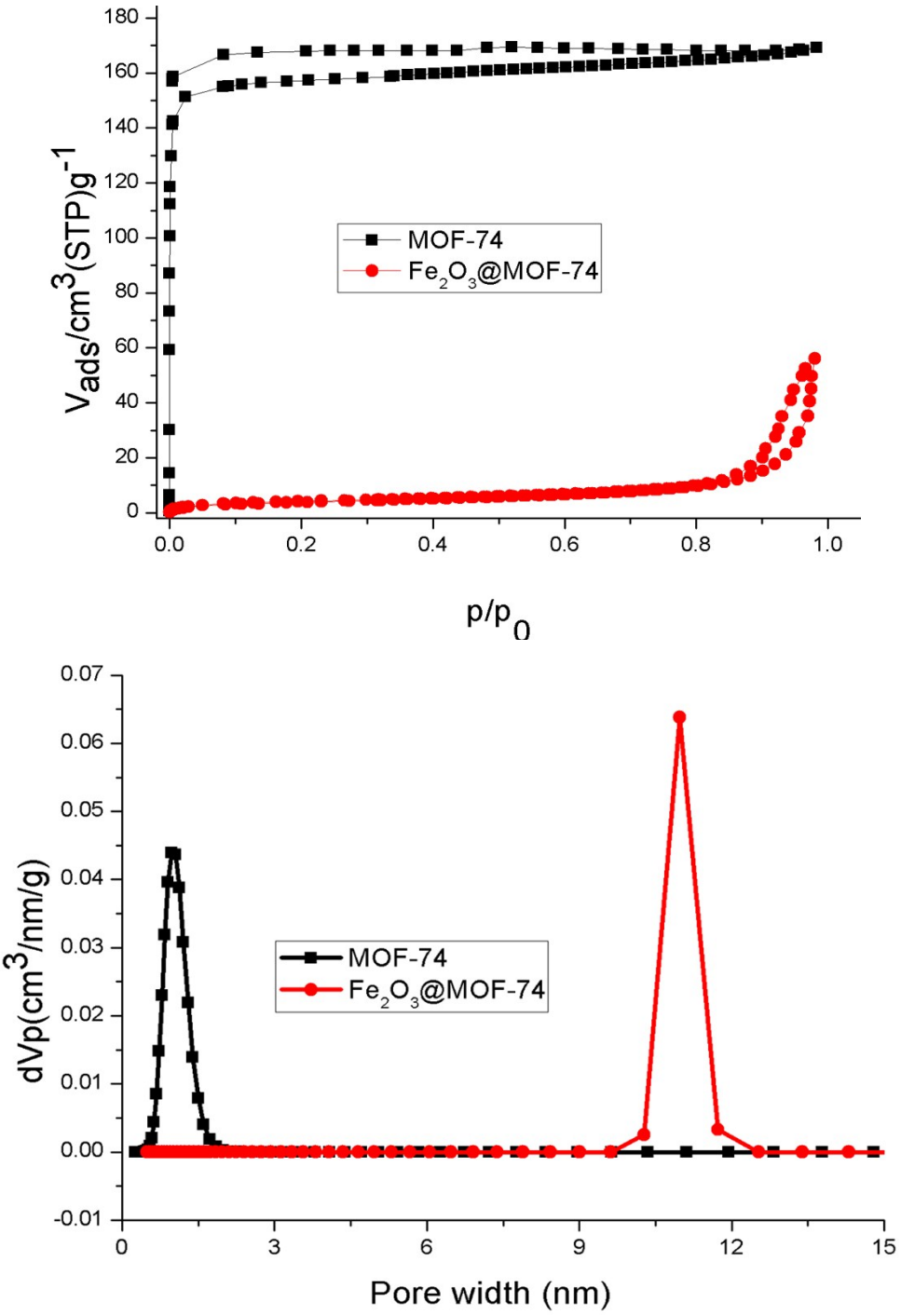

Fig. S17 Nitrogen physisorption isotherm of as-synthesized UTSA-74 and Fe_2O_3@UTSA-74 samples. The sample was pretreated at 80°C under vacuum for 12 h. The BET surface area and Langmuir surface area for UTSA-74 and Fe_2O_3@UTSA-74 is 830/996 m^2/g and 528.4/681.1 m^2/g, respectively. UTSA-74 gives aperture around 0.8 nm, whereas Fe_2O_3@UTSA-74 creates a microporous-mesoporous form with microprous aperture around 0.7 nm and mesoporous aperture around 5.3 nm.

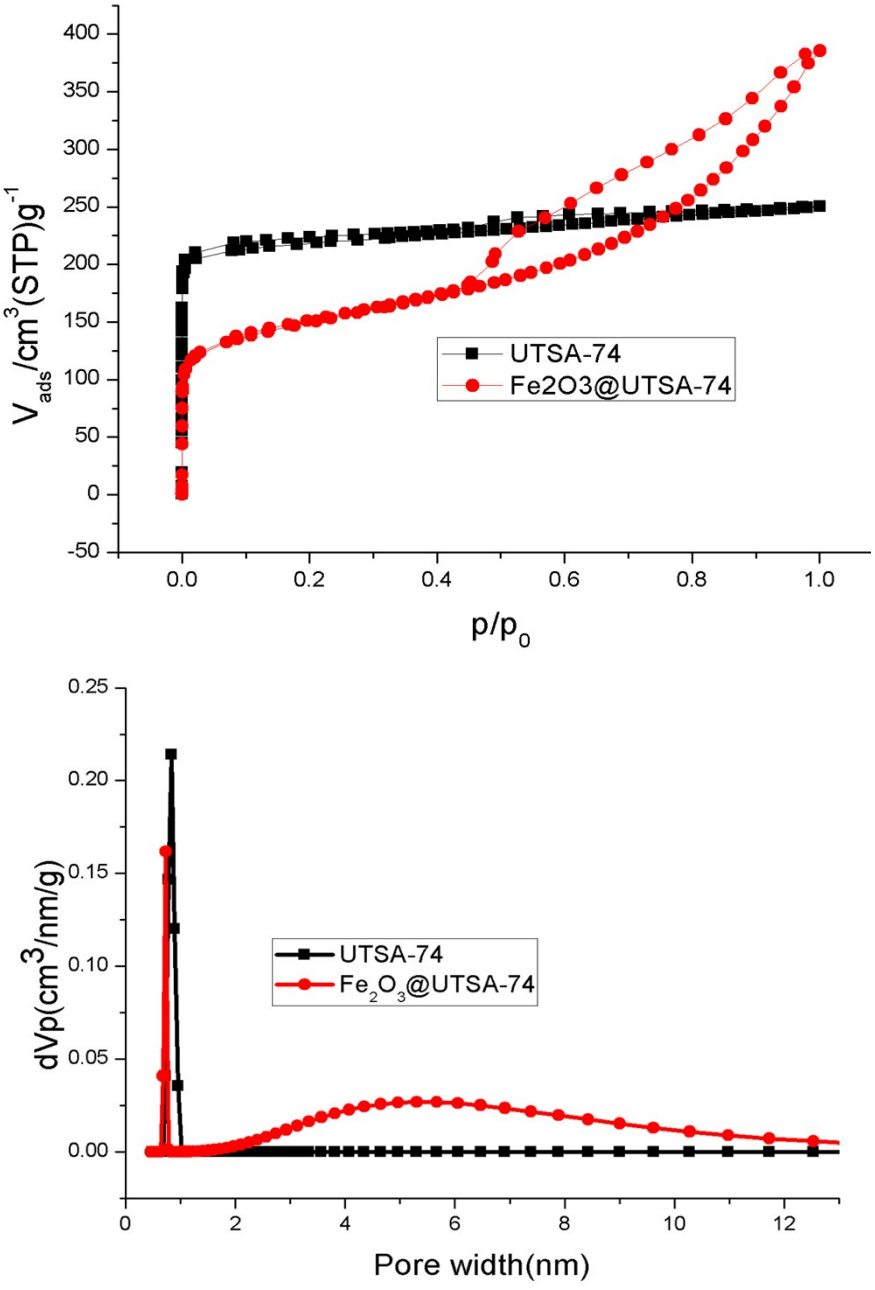

Fig. S18 Nitrogen physisorption isotherm of Fe_2O_3@Mg(DHT)$(DMF)_2$ samples. The sample was pretreated at 80°C under vacuum for 12 h. The BET surface area and Langmuir surface area for Fe_2O_3@Mg(DHT)$(DMF)_2$ is 32.2/41.2 m^2/g, giving mesoporous form with aperture around 8.6 nm. By contrast, the as-synthesized Mg(DHT)$(DMF)_2$ samples is nonporous, thus, the mesoporous form is contributed by Fe_2O_3.

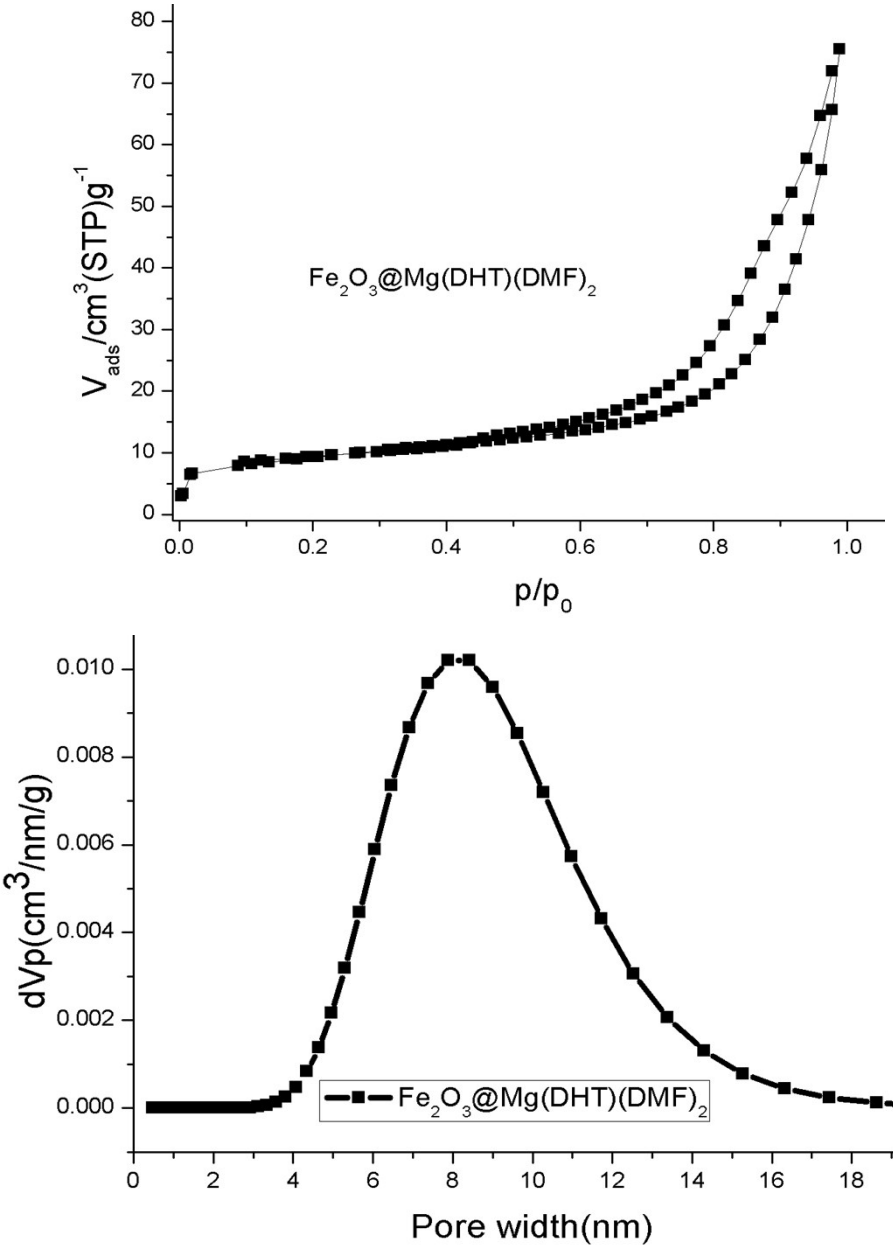

Fig. S19 Nitrogen physisorption isotherm of as-synthesized UiO-66(OH)$_2$ and Fe_2O_3@ UiO-66(OH)$_2$ samples. The sample was pretreated at 80°C under vacuum for 12 h. The BET surface area and Langmuir surface area for UiO-66(OH)$_2$ and Fe_2O_3@UiO-66(OH)$_2$ is 561.4/672.5 m^2/g and 195.1/264.7 m^2/g, respectively. UiO-66(OH)$_2$ gives aperture around 0.85 nm, whereas Fe_2O_3@ UiO-66(OH)$_2$ gives aperture around 0.68 nm.

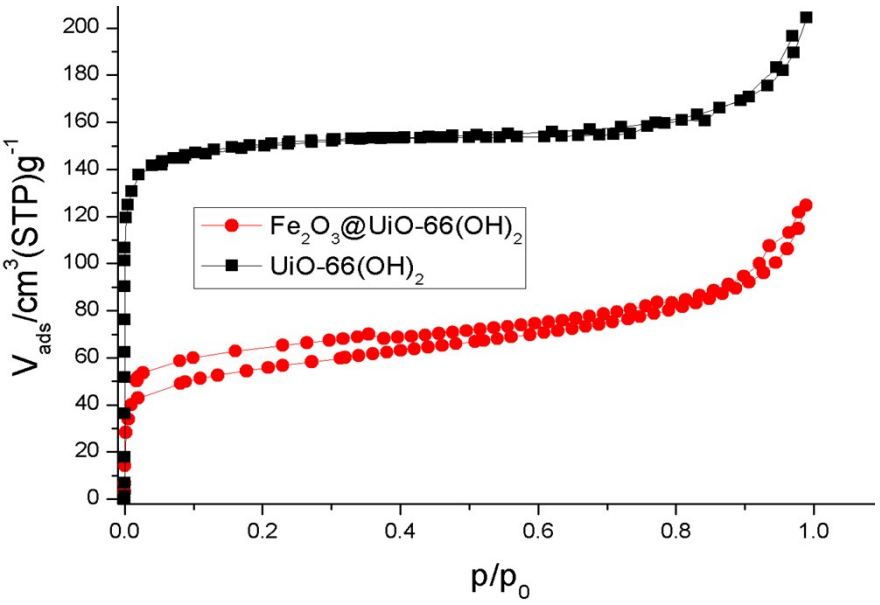

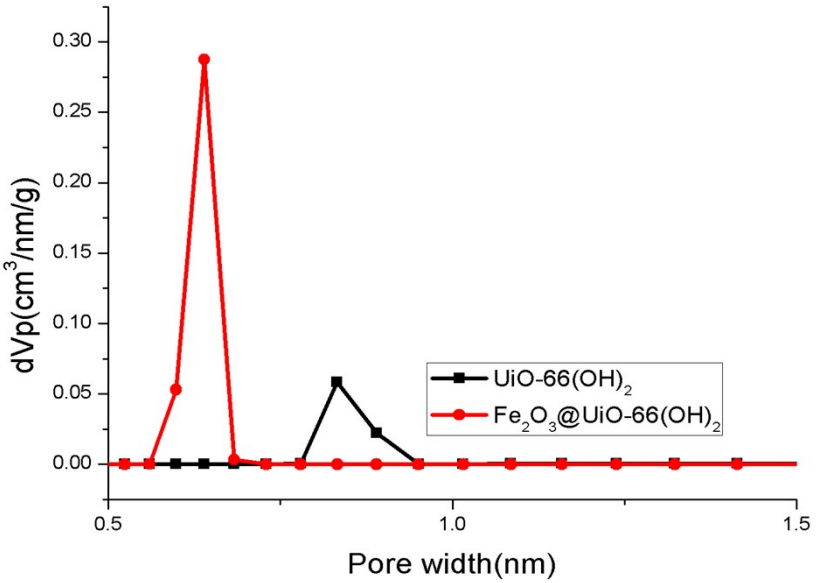

Fig. S20 Nitrogen physisorption isotherm of as-synthesized UiO-66(OH) and Fe_2O_3@ UiO-66(OH) samples. The sample was pretreated at 80°C under vacuum for 12 h. The BET surface area and Langmuir surface area for UiO-66(OH) and Fe_2O_3@UiO-66(OH) is 824/1025 m^2/g and 505.6/613.7 m^2/g, respectively. UiO-66(OH) gives aperture around 0.81 nm, whereas Fe_2O_3@ UiO-66(OH) gives aperture around 0.75 nm.

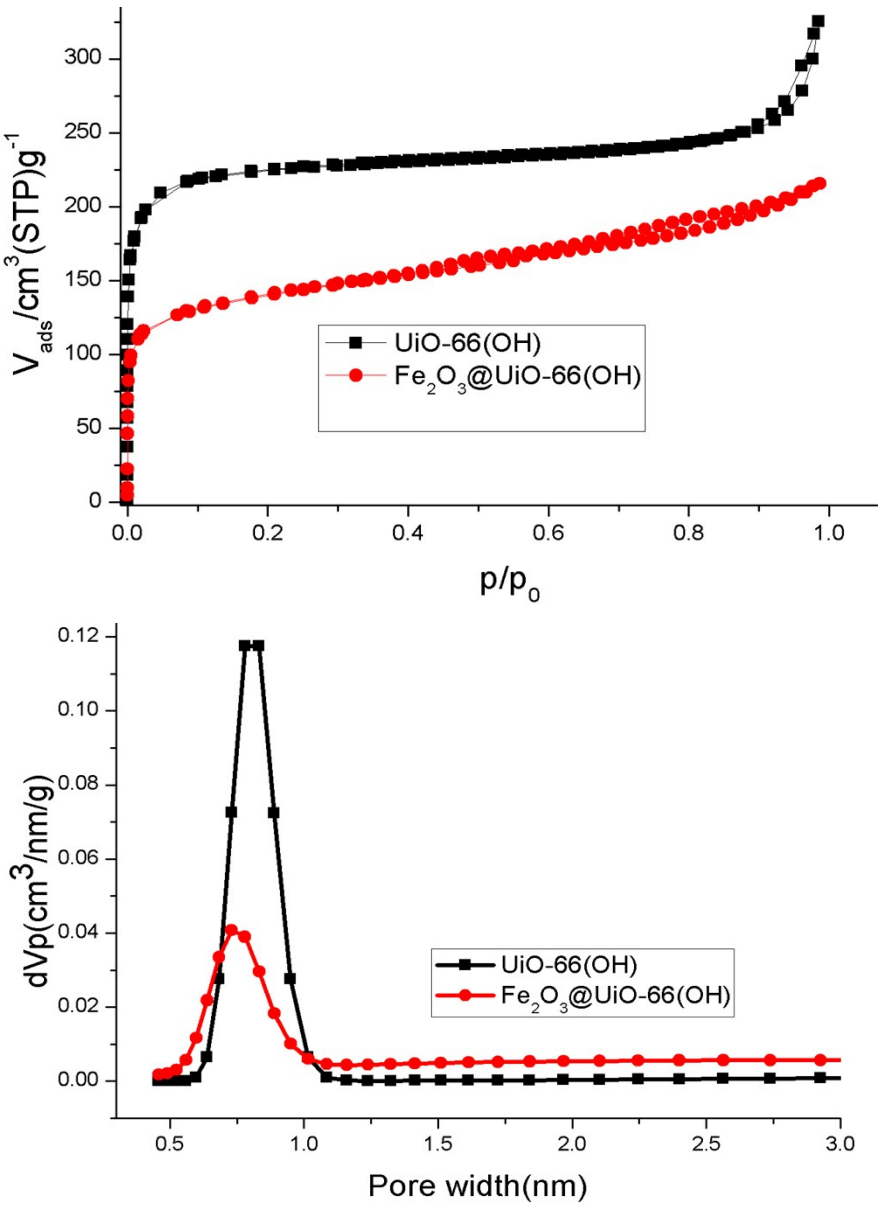

Fig. S21 The magnetic hysteresis of Fe_2O_3@MOF-74 at 300K, where very small magnetic hysteresis is observed, indicative of very weak ferromagnetic properties of Fe_2O_3@MOF-74 at 300K. This is well consistent with the experiment result that the Fe_2O_3@MOF-74 samples can be enriched by magnet.

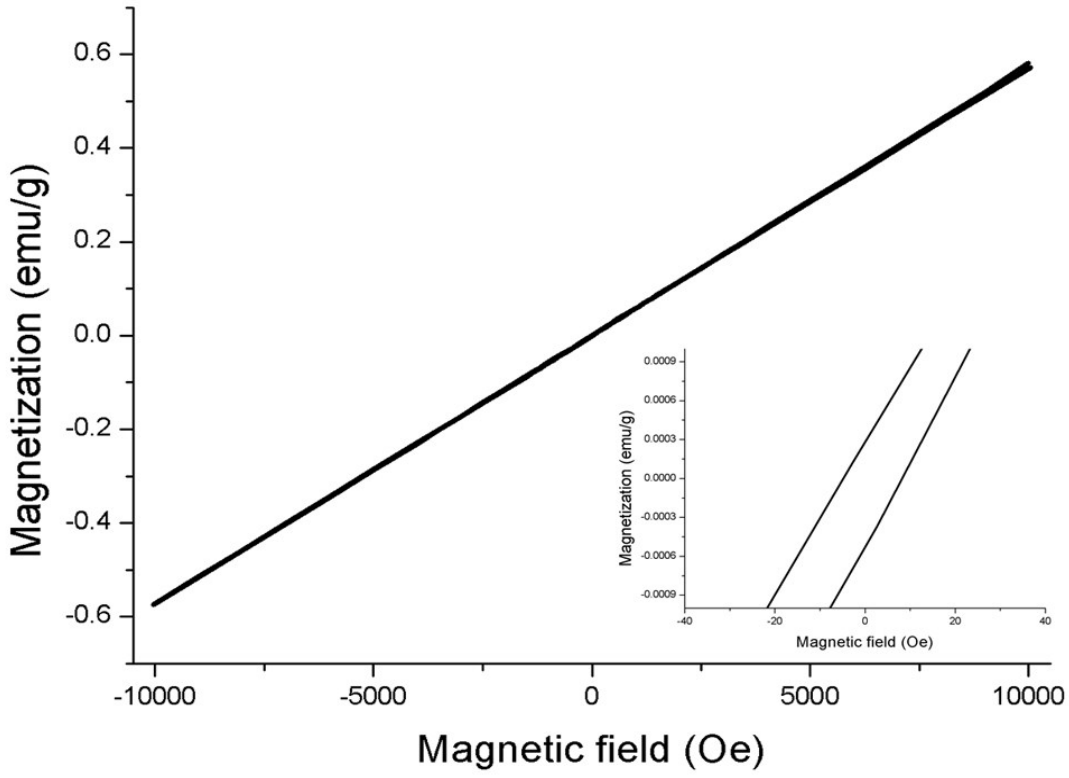

Fig. S22 The magnetic hysteresis of Fe_2O_3@UTSA-74 at 300K, where small magnetic hysteresis is observed, indicative of weak ferromagnetic properties of Fe_2O_3@UTSA-74 at 300K. This is well consistent with the experiment result that the Fe_2O_3@UTSA-74 samples can be enriched by magnet.